F-18 WING ROCK CONSIDERATIONS

L. E. Ericsson

Engineering Consultant

Mountain View, California, USA

Abstract

In tests of the F/A-18 aircraft, wing rock was observed in laminar subscale tests as well as in full-scale flight, whereas wind tunnel tests at an intermediate Reynolds number showed no wing rock. An analysis has been performed to try to pinpoint the flow physics behind this chain of events.

Nomenclature

b	wing span
d	maximum body diameter
d_N	maximum nose diameter
l'	sectional lift, coefficient $c_l = l'/q_\infty(\pi d^2/4)$
l	rolling moment, coefficient $C_l = l/q_\infty S b$
L	length of LEX
L_N	nose length
N	normal force, coefficient $C_N = N/q_\infty(\pi d^2/4)$
p	body roll rate
q_∞	free stream dynamic pressure, $= \rho_\infty U_\infty^2/2$
S	reference area, projected wing area
t	time
Δt	time lag
U_∞	free stream velocity
U_W	moving wall velocity
x	axial body coordinate
Y	side force, coefficient $C_Y = Y/q_\infty(\pi d^2/4)$
α	angle of attack
Δ	increment
ϕ	roll angle
$\dot{\phi}$	roll rate, $= \partial\phi/\partial t$
ϕ_S	azimuth of body strake
θ_A	apex half angle

Subscripts

1,2.3	numbering subscripts
∞	free stream conditions

Introduction

In a recent AGARD-FDP special course on Aircraft Dynamics at High Angles of Attack, held at NASA Langley Research Center, 8-11 April, 1991, R.C.Nelson, University of Notre Dame, showed a film clip of F-18 wing rock at high angles of attack.[1] Both the full scale flow visualization and the one with a small model in a water tunnel showed a very extensive interaction between forebody and leading-edge-extension(LEX)vortices, resulting in large-amplitude wing rock[1,2](Fig. 1). At the repetition of the course at the von Karman Institute in Belgium, Nelson revealed that testing a larger F-18 model in a wind tunnel at NASA Langley Research Center, at a much higher Reynolds number than in the Notre Dame tunnel test, L.T.Nguyen et al had not observed any wing rock at all. This was an illustration of the difficulties discussed in Ref. 3, Nelson thought. The situation is the opposite of that encountered earlier in tests of a generic aircraft model.[4] In this case, tests at NASA Langley R C (in the same tunnel and at a similar Reynolds number) showed wing rock to exist (Fig. 2), whereas it would not occur in laminar flow[5,6], and would be much less severe at full scale Reynolds numbers[7]. The present paper presents a separated-flow hypothesis that can explain these rather unusual experimental results.

Analysis

The high-alpha forebody flow on a model of F/A-18 was investigated in conjunction with a test of forebody blowing[8](Fig. 3). The flow visualization for no blowing shows that the forebody vortices are symmetric at $\alpha = 50^o$ but become asymmetric at $\alpha = 60^o$ with the lower of the vortices , the one that is not "lifted-off", staying close to the nose contour (Fig. 4). In another test[9,10] flow visualization showed spiral breakdown of the LEX vortex (Fig. 5).

Based upon the flow pictures in Figs. 4 and 5, one can construct the conceptual forebody-LEX vortex geometry shown in Fig. 6, explaining the interaction described by Nelson[1]. In the film clip he showed, one could see how one of the forebody vortices at a high angle of attack would dip down to interact with the LEX vortex on that side of the body. That started the wing-rocking action, with the forebody-LEX vortex interaction alternating between the two sides. Section A-A in Fig. 6 illustrates how the LEX vortex, after spiral vortex breakdown, would generate a velocity field that "drags" down the forebody vortex, starting a spiraling interaction by the two vortices. On the Swedish "Draken" aircraft a similar interaction between the inner and outer delta wing leading-edge vortices caused a sudden unloading of the vortex-induced lift on the outer, main delta wing, resulting in a pitch-up moment that greatly exceeded the plane's control capability[11] (Fig. 7). A similar interaction between the vortex from the rounded leading edge of the "wing glove", at the wing root, and the vortex from the sharp leading edge of the main wing caused bending oscillations of the 67.5 deg swept wing of a large military aircraft[12,13]. In the present case, the interaction between forebody and LEX vortices is also likely to result in similar vortex lift-off. As a result, much of the beneficial effect of the LEX-vortex, i.e., the delay of flow separation on the main wing due to the vortex-induced flow field, is lost. It remains to demonstrate how this forebody-LEX vortex interaction can cause the observed wing rock.

Moving Wall Effect

Moving wall effects[14] generate wing rock through their influence on the forebody cross flow separation and associated vortex shedding[5,6]. They are very dependent upon the cross flow Reynolds number in regard to the nature of their induced aerodynamic effects. This is illustrated by Magnus lift measurements on a rotating circular cylinder[15] (Fig. 8). For laminar flow conditions (curve f in Fig. 8 for $U_W/U_\infty < 0.3$), positive Magnus lift is generated. This is mainly the result of the separation delay on the top side through the downstream moving wall effects. In contrast, at critical flow conditions, negative Magnus lift is generated by the promotion of transition on the bottom side through upstream moving wall effects, causing a change from the subcritical to the supercritical type of flow separation, e. g. at $Re = 0.128 \times 10^6$ and $U_W/U_\infty \geq 0.3$ (curve f in Fig. 8). The negative Magnus lift reaches its maximum magnitude when the cross flow conditions are of the critical type already in the static case (curves j, k, and l in Fig. 8) .

In the analysis in Refs. 5 and 6 of the wing rock of a generic aircraft observed experimentally[4] (Fig. 2), it was assumed that critical cross flow conditions existed on the forebody. The Reynolds number based upon the diameter of the cylindrical aft body in the test[4] was $Re = 0.26 \times 10^6$, i. e., in the critical Re-regime[15] (Fig. 8). Thus, the cross flow over the nose and nose shoulder will be in the critical region, and the scenario in Fig. 9 can be visualized. At $t = t_1$, the adverse upstream moving wall effect on the forebody cross flow causes boundary layer transition to occur earlier, as illustrated in the figure. The effect is similar to that of changing the separation from the subcritical to the critical or supercritical type (Fig 8). In the absence of time lag effects, the vortex geometry sketched at $t = t_1$ would result. Due to time lag effects similar to those for slender wing rock[16], this vortex geometry is not realized until $t = t_2 = t_1 + \Delta t$. For simplicity, only the vortex closest to the body is shown at t_2 , as it indicates the direction of the vortex-induced downwash and the resulting rolling moment.

At $t = t_3$, when the roll rate reaches its maximum in the opposite direction, another forebody switch of the flow separation asymmetry occurs. Because of the time lag effect, the vortex geometry influencing the now horizontal wing has not changed, but is the same as at $t_2 = t_1 + \Delta t$, in agreement with the flow pictures in Ref. 4. During the time lag Δt, the vortex-induced rolling moment drives the rolling motion, generating the observed wing rock[4]. This is illustrated in Fig. 10. The rolling moment increment ΔC_l , induced by the switch of forebody vortex asymmetry, is statically stabilizing. The roll angle $\dot{\phi}\Delta t$, generated by the time lag Δt, discussed earlier in connection with Fig. 9, makes ΔC_l have a dynamically destabilizing effect.

F-18 Wing Rock

Using the information in Figs. 4 through 6, the flow sketch corresponding to Fig. 9 looks for the subscale test of the F/A-18 model as is shown in Fig. 11. The downstream moving-wall effect delays flow separation for laminar flow conditions ($U_W/U_\infty < 0.3$ for curve f in Fig. 8). In Fig. 11 the aerodynamic spring needed for the oscillatory wing-rock motion is provided by the rolling moment generated by the loss of lift on the main wing through the vortex interaction. (Note that the direction of the forebody rotation is opposite in Fig. 11 to what it is in Fig. 9). As in the case of the generic aircraft model in Fig. 9, there is a time-lag Δt after the rotation of the forebody has changed before the vortex interaction occurs. This generates the rolling moment that drives the wing-rock motion.

The wing rock amplitude of F/A-18, observed in flight and measured at low Reynolds numbers in wind tunnel tests[2], shows the amplitude to increase with angle of attack, from approximately 3 deg at $\alpha = 30^o$ to a maximum of slightly more than 20 deg at $\alpha = 45^o$ (Fig. 1). When the angle of attack is increased further, the limit cycle amplitude decreases rapidly. The flow physics behind these data trends will be discussed next. From Fig. 6 one obtains the estimate $L_N/d_N \approx 2.5$. For a tangent-ogive nose the corresponding apex half angle is $\theta_A = 23.7^o$, indicating that static asymmetric forebody vortices should start developing when $\alpha > 2\,\theta_A = 47.4$ deg[17]. This is in good agreement with the flow visualization results in Fig. 4, showing that asymmetric forebody vortices started occurring at $\alpha > 50^o$. It is also in agreement with the data trend in Fig. 1. As discussed in Ref. 18 in connection with test results for a spinning nose tip[19], the moving wall effect is largest just before natural separation asymmetry occurs, at $\alpha \approx 45^o$ in Fig. 1. At that point, the symmetric flow separation is easiest to perturb to change the symmetric vortex pattern to an asymmetric one in the desired direction. The rapid decline of the wing rock amplitude at higher angles of attack reflects the fact that the moving wall effect now has to overcome the natural, static separation asymmetry. Also contributing to this data trend is that the static vortex breakdown (for the non-rolling aircraft) occurs closer and closer to the LEX-apex, leaving less room for the vortex interaction because of the presence of the cockpit (See Section B-B in Fig. 6).

The data trend for $\alpha < 45^o$ in Fig. 1 is the expected one. Symmetric forebody flow separation should start at $\alpha > \theta_A = 23.7^o$ (Ref. 17). The moving wall effect will have more and more difficulty in trying to perturb the symmetric flow separation farther and farther away from the "trigger point" $\alpha = 45^o$. The nose "microasymmetry" has the same difficulty[17], as is demonstrated by the static

experimental results for an $L_N/d_N = 3.5$ pointed ogive[20] (Fig. 12).

The agreement between the wind tunnel test and free flight results in Fig. 1 appears at first rather surprising. However, it is well known[17] that the side forces generated by asymmetric forebody flow separation are of similar magnitudes for laminar and turbulent flow conditions, as is demonstrated by the experimental results[21] in Fig. 13. When comparing flight data with wind tunnel measurements in Fig. 1, one has to account for the bearing friction present in the wind tunnel test. It has been observed to have a very significant effect on the wing-rock boundary for an 80 deg delta wing[22] (Fig. 14). The predicted boundary for free flight[23] shows wing rock to start at $\alpha \approx 20^o$. In a wind tunnel test with a regular bearing[24], wing rock started at $\alpha \approx 27^o$. However, when the same air bearing was used as in the F/A-18 test[2], wing rock started already at $\alpha \approx 22^o$ (Ref. 25), only 2 deg later than in free flight. Zero-shifting the wind tunnel data 2 deg to account for the effect of the air bearing still makes a significant difference (the dashed line in Fig. 15). The comparison of these adjusted wind tunnel results with the free flight estimate is in basic agreement with the comparison in Fig. 13 between laminar and turbulent side force data. However, one must also compare the laminar and turbulent moving wall effects.

Figure 16 shows the Magnus lift measured by Swanson[15] on a rotating circular cylinder. In the laminar, subcritical case (Fig. 16a), the Magnus lift is generated mainly by the downstream moving wall effect on the top side, which moves the flow separation from the subcritical towards the supercritical position. On the bottom side the flow separation is occurring forward of the lateral meridian already in the static case, and the upstream moving wall effect does not have much leverage for its separation-promoting action. However, in the turbulent, supercritical case (Fig. 16b), the situation is reversed. The main effect is that of the upstream moving wall effect on the bottom side, which promotes flow separation, moving it from the supercritical towards the subcritical position. The downstream moving wall effect on the top side has very limited possibility to cause further delay of the already supercritical flow separation. Thus, the difference in Magnus lift between laminar and turbulent flow conditions is mainly the result of the difference between the capability of the moving wall effect to delay laminar flow separation and promote turbulent separation. The difference in Magnus lift slopes, the laminar one being only 3/8 of the turbulent one, reflects the fact that it is much more difficult to delay than to promote flow separation.

In the present case of interest the laminar flow separation is delayed by the moving wall effect (Fig. 17a) whereas the turbulent separation is promoted (Fig. 17b). The result is a forebody vortex pair that looks very similar. This similarity is facilitated greatly by the process illustrated in Fig. 18 by experimental results for a 5 caliber pointed tangent-ogive[20]. When one vortex lifts up as a result of asymmetric cross flow separation, the other vortex moves inboard under the lifted vortex. This occurs even under steady, symmetric cross flow conditions, caused by the nose microasymmetry[17] (Fig. 12), resulting in a side force and an increased normal force. Thus, regardless of how the asymmetric cross flow separation is established, the resulting asymmetric loads and vortices are very similar, as is illustrated in Fig. 13 for the static case and in Fig. 15 for the case of the F-18 wing rock.

Reynolds Number Effects

Based upon the results in Fig. 8, one expects the effect of rotation on the flow separation and associated vortex geometry to switch if the Reynolds number is increased to fall in the critical range. In that case, the forebody-LEX vortex interaction would be statically destabilizing but dynamically stabilizing. Thus, no wing rock should occur. That is exactly what was observed when the F/A-18 model was tested[26] at roughly the same cross-flow Reynolds number for the forebody as in the case of the generic aircraft model[4]. However, when the forebody of the F/A-18 model was provided with small strakes, at $\varphi_S = \pm 40$ degrees azimuth from the bottom meridian, wing rock did occur. The likely reason for this is that the strakes caused early, localized, transitional flow separation and reattachment, resulting in a delay of the final, turbulent flow separation (Fig. 19). A similar supercritical type of flow separation would probably also result if the strakes were substituted by boundary layer trips[17].

It is to be expected that Reynolds number effects can be large close to the critical flow region. However, what could cause the large effect of Reynolds number observed in the F-18 wing rock test[2], performed under laminar flow conditions (Fig. 20)? A compilation of experimental results for the breakdown of the LEX vortex on the F-18 aircraft[10] (Fig. 21) reveals the source of this Reynolds number sensitivity of the wing rock. At $Re = 5500$, the water tunnel data show that at $\alpha = 35^o$ the vortex breakdown occurs at $x/L > 0.55$ compared to $x/L < 0.45$ for $Re > 1.6 \times 10^6$. Thus, the likely reason for the large effect of Reynolds number below $Re = 30000$ in Fig. 20 is that the spiraling LEX vortex aft of the breakdown moves back and below the forebody vortex (See Fig. 6), increasing the distance between the vortices, weakening their interaction as the Reynolds number is decreased.

Conclusions

A brief analysis of recent experimental results for the F/A-18 aircraft has led to the following conclusions:

1. The at first look apparently anomalous experimental results for the wing rock of the F/A-18 aircraft can be explained by extending the analysis performed earlier for the wing rock of a generic aircraft model. The main change is that instead of inducing downwash on the main wing, the forebody vortex in the present case interacts with the LEX vortex, controlling its lift generation on the main wing.
2. The results provide one more example of the fact that dynamic simulation of separation-induced self-excited oscillations in subscale tests is not possible unless the full-scale Reynolds number is simulated. One encouraging result of the present analysis is that it indicates that even in the presence of so called moving wall effects analytic extrapolation to full-scale vehicle dynamics from subscale tests may be possible, provided that the fluid mechanics involved are well understood.

References

1. Nelson, R. C., "Unsteady Aerodynamics of Slender Wings", Paper 1, AGARD-R-776, April 1991. (The F-18 wing-rock results were only presented orally.)

2. Quest, T., Nelson, R. C., and Fisher, D. F., "A Study of High-Alpha Dynamics and Flow Visualization for a 2.5 % Model of the F-18 HARV Undergoing Wing Rock," AIAA Paper 91-3267-CP, Sept. 1991.

3. Ericsson, L.E., "Effects of Transition on Wind Tunnel Simulation of Vehicle Dynamics", Progress in Aerospace Sciences, Vol. 27, 1990, pp. 121-144.

4. Brandon, J. M. and Nguyen L.T., "Experimental Study of Effects of Forebody Geometry on High Angle of Attack Stability", Journal of Aircraft, Vol. 25, July 1988, pp. 591-597.

5. Ericsson, L.E., "Wing Rock Generated by Forebody Vortices", Journal of Aircraft, Vol. 26, Feb. 1989, pp. 110-116.

6. Ericsson, L. E. and Mendenhall, M. R., "On Forebody-Induced Wing Rock," AIAA Paper 94-0167, Jan. 1994.

7. Ericsson, L. E., "Prediction of High-Alpha Vehicle Dynamics", ICAS-90-3.6.1, Sept. 1990.

8. Malcolm, G. N., "Forebody Vortex Control", Paper 6, AGARD-R-776, April 1991.

9. Hebbar, S. K., Platzer, M. F., and Cavazos, O. V., "A Water Tunnel Investigation of the Effects of Pitch Rate and Yaw on LEX Generated Vortices of an F/A-18 Fighter Aircraft Model", AIAA Paper 91-0280, Jan. 1991

10. Cavazos, O.V.Jr., "A Flow Visualization Study of LEX Generated Vortices on a Scale Model of a F/A-18 Fighter Aircraft at High Angles of Attack", M.S. Thesis, Naval Postgraduate School, Monterey, California, June 1990.

11. Reding, J. P. and Ericsson, L. E., "Review of Delta Wing Space Shuttle Vehicle Dynamics," NASA CR-115357, Oct. 1971.

12. Ericsson, L. E., "Vortex-Induced Bending Oscillation of a Swept Wing," Journal of Aircraft, Vol. 24, March 1987, pp. 195-202.

13. Dobbs, S. K., Miller, G. D., and Stevenson, J. R., "Self-Induced Oscillating Wind Tunnel Test of a Variable Sweep Wing," AIAA Paper 85-0739, April 1985.

14. Ericsson, L. E., "Moving Wall Effects in Unsteady Flow", Journal of Aircraft, Vol. 25, No. 11, Nov. 1988, pp. 977-990.

15. Swanson, W. M., "The Magnus Effect: A Summary of Investigations to Date", Journal of Basic Engineering, Vol. 83, Sept. 1961, pp. 461-470.

16. Ericsson, L. E., "The Fluid Mechanics of Slender Wing Rock", Journal of Aircraft, Vol.21, May 1984, pp. 322-328.

17. Ericsson, L. E. and Reding, J. P., "Asymmetric Flow Separation and Vortex Shedding on Bodies of Revolution," Tactical Missile Aerodynamics: General Topics, Vol. 141, Progress Astro. and Aero. Series, M. J. Hemsch editor, 1992, pp. 391-452.

18. Ericsson, L. E., "Unsteady Separation on Slender Bodies at High Angles of Attack," Journal of Spacecraft and Rockets, Vol. 30, Nov.-Dec. 1993, pp. 689-695.

19. Fidler, J. E., "Active Control of Asymmetric Vortex Effects," Journal of Aircraft, Vol. 18, April 1981, pp. 267-272.

20. Keener, E. R., Chapman, G. T., Cohen, L., and Taleghani, J. , " Side Forces on Forebodies at High Angles of Attack and Mach Numbers from 0.1 to 0.7. Two Tangent Ogives, Paraboloid and Cone," NASA TM X-3438, Feb. 1977.

21. Lamont, P. J., "The Complex Asymmetric Flow Over a 3.4D Ogive Nose and Cylindrical Afterbody at High Angles of Attack," AIAA Paper 82-0053, Jan. 1982.

22 Ericsson, L. E., "Slender Wing Rock Revisited," Journal of Aircraft, Vol. 30, May-June 1993, pp. 352-356.

23. Ericsson. L. E. and King, H. H. C., "Rapid Prediction of High-Alpha Unsteady Aerodynamics of Slender-Wing Aircraft," Journal of Aircraft, Vol. 29, Jan.-Feb. 1992, pp. 85-92.

24. Nguyen, L. T., Yip, L. P., and Chambers, J. R., "Self-Induced Wing Rock of Slender Delta Wings," AIAA Paper 81-1883, Aug. 1981.

25. Arena, H. S. Jr., Nelson, R. C., and Schiff, L. B., "An Experimental Study of the Nonlinear Dynamic Phenomenon known as Wing Rock," AIAA Paper 90-2812-CP, Aug. 1990.

26. Nguyen, L. T., Private Communication, April 30, 1991.

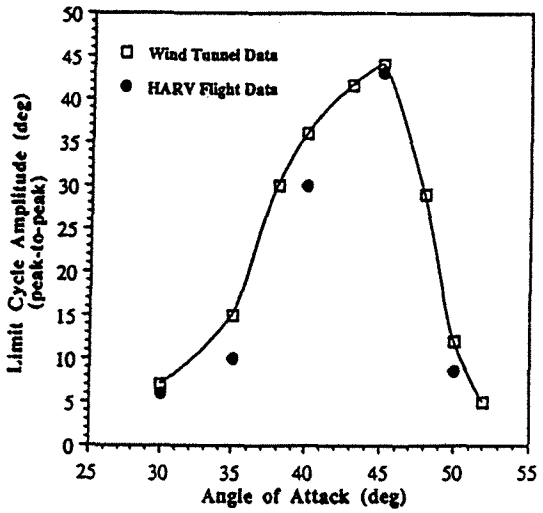

Fig. 1. Wing rock of the F-18 HARV aircraft[2].

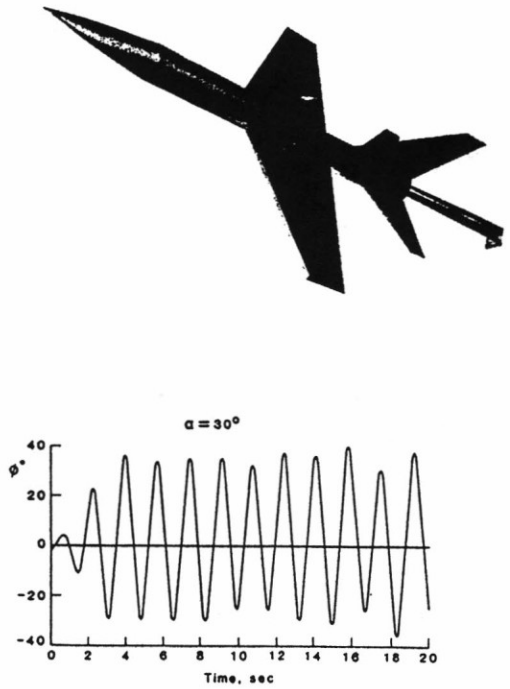

Fig. 2. Wing rock build-up at α = 30 deg of a generic aircraft model[4].

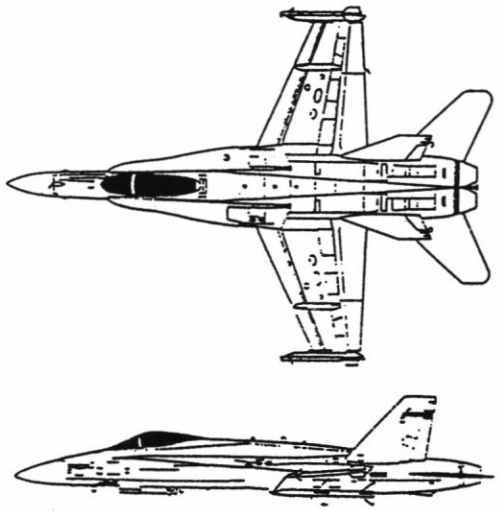

Fig. 3. F/A-18 aircraft model[8].

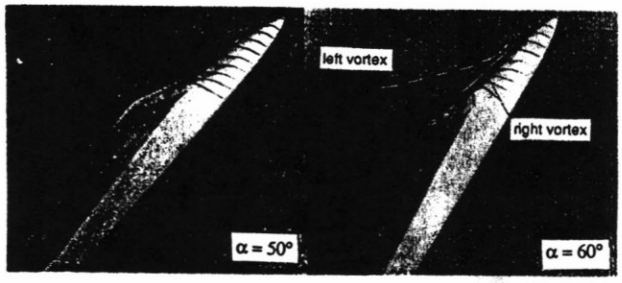

Fig. 4. F/A-18 forebody flow visualization at α = 50 and 60 deg[8].

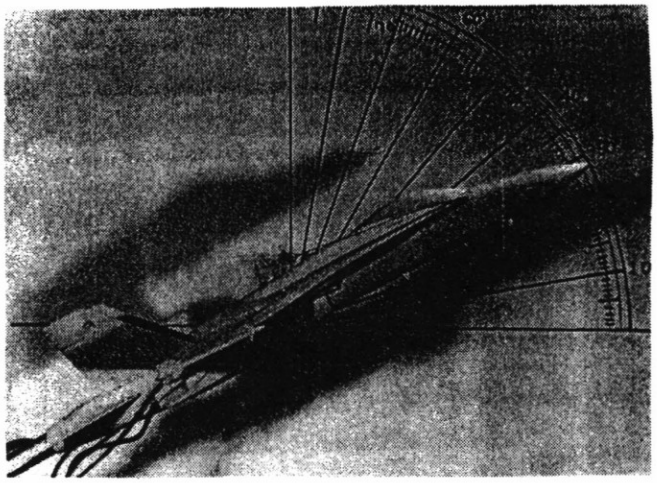

Fig. 5. LEX-vortex flow, static case, α = 29 deg[10].

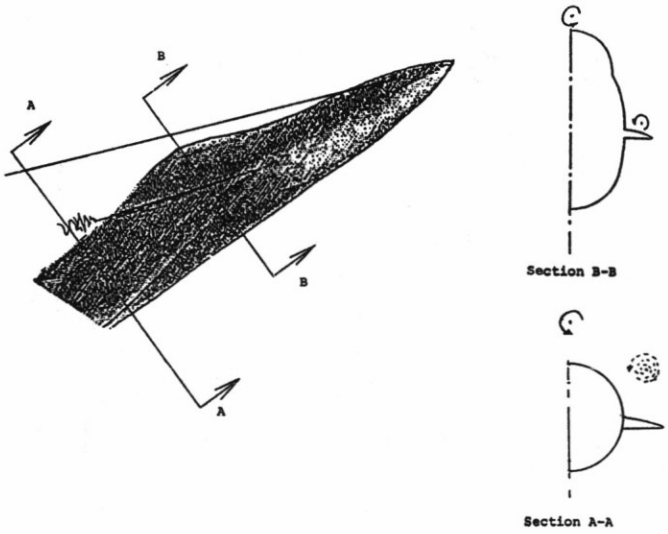

Fig. 6. Conceptual flow geometry for LEX-forebody vortex interaction.

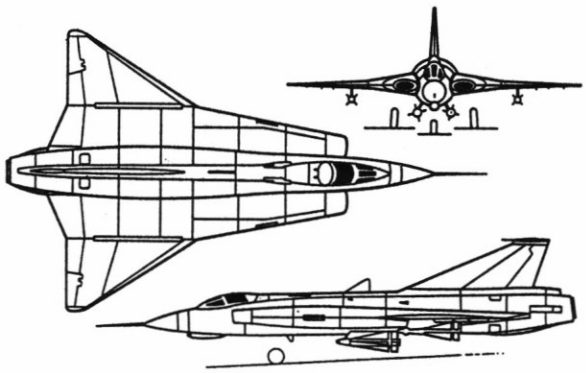

Fig. 7. Swedish aircraft "DRAKEN" (Ref. 11).

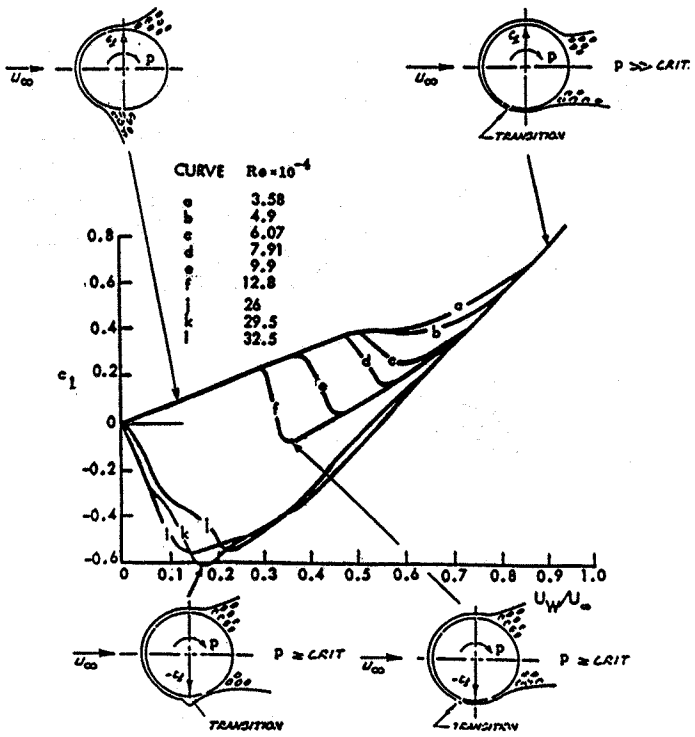

Fig. 8. Magnus lift characteristics for initially subcritical (laminar) flow conditions[15].

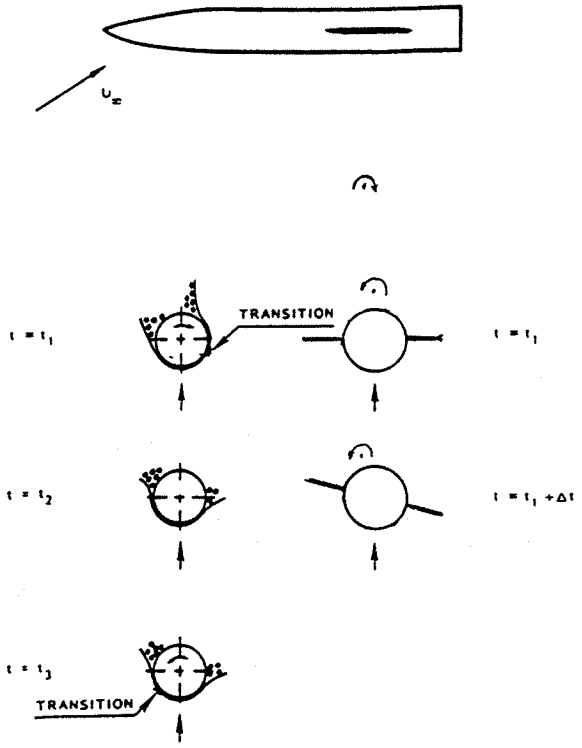

Fig. 9 Conceptual flow mechanism for forebody-induced wing rock[5].

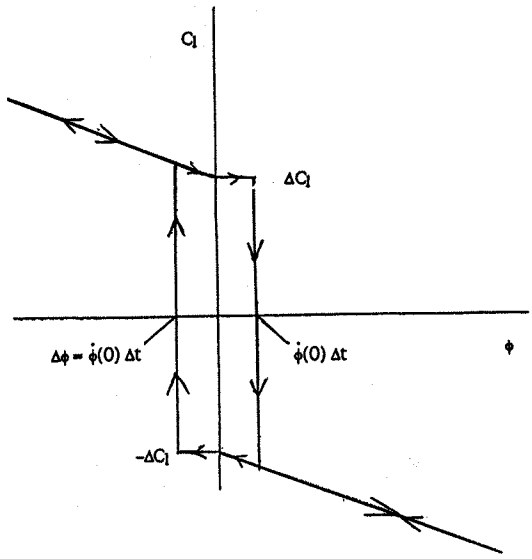

Fig. 10. Conceptual undamping hysteresis induced by time lag[6].

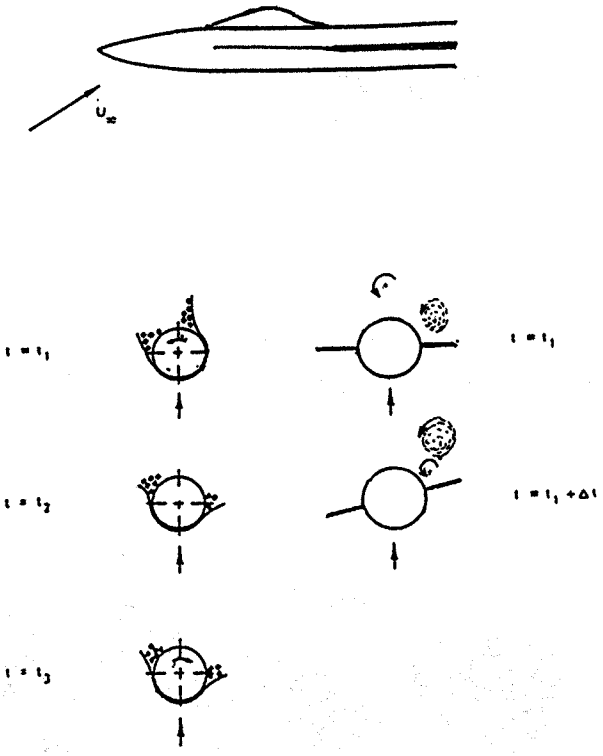

Fig. 11. Conceptual flow mechanism for LEX-forebody vortex interaction.

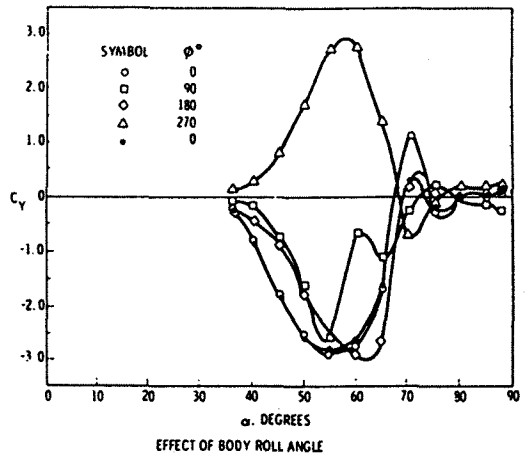

EFFECT OF BODY ROLL ANGLE

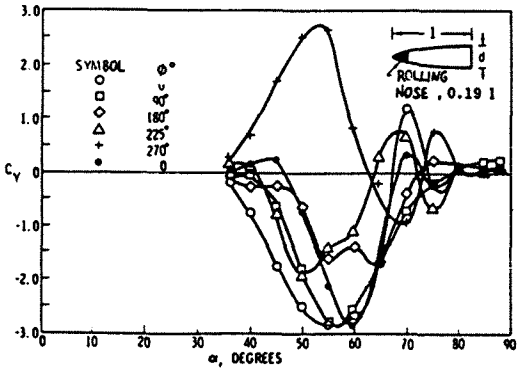

EFFECT OF NOSE ROLL ANGLE

Fig. 12. Effect of roll angle on the side force on an L_N/d_N = 3.5 pointed ogive at M = 0.25 and Re = 0.8 x10^6 (Ref. 20).

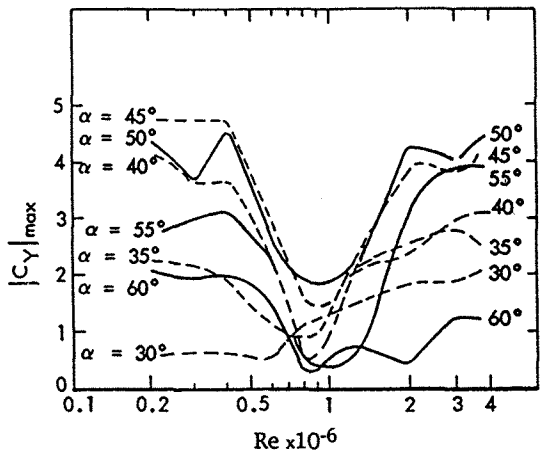

Fig. 13. Effect of Reynolds number on maximum asymmetric side force on an l_N/d_N = 3.4 ogive-cylinder[21].

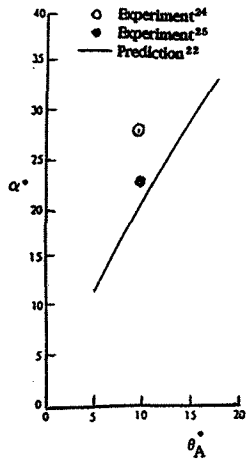

Fig. 14. Wing rock boundary for 80 deg delta wings.

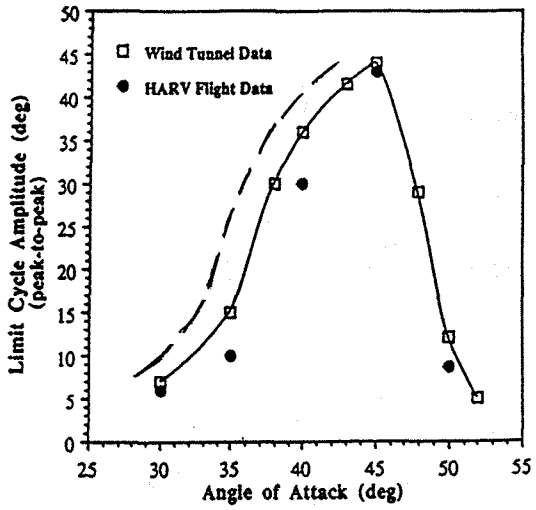

Fig. 15. Wing rock characteristics for the F/A-18 model adjusted for the effect of bearing friction.

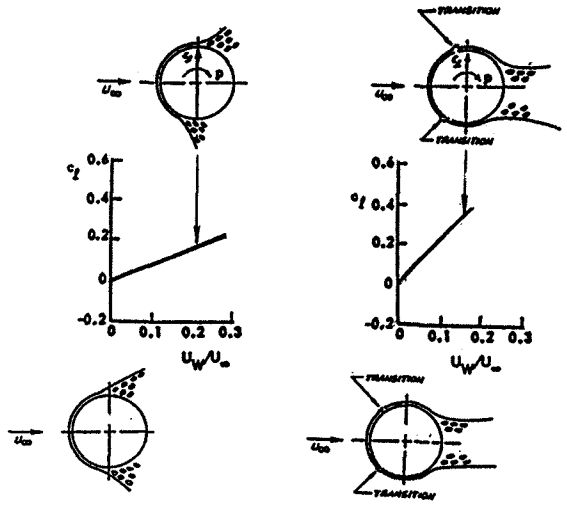

a) Laminar, subcritical flow conditions, Re < 10^5.

b) Turbulent, supercritical flow conditions, Re > 5 x 10^5.

Fig. 16. Laminar and turbulent Magnus lift of a circular cylinder[15].

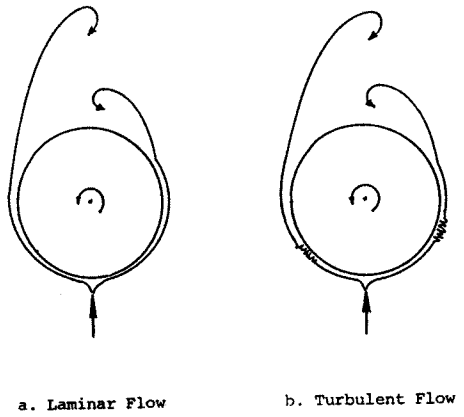

Fig. 17. Conceptual asymmetric forebody vortex geometries for laminar and turbulent flow.

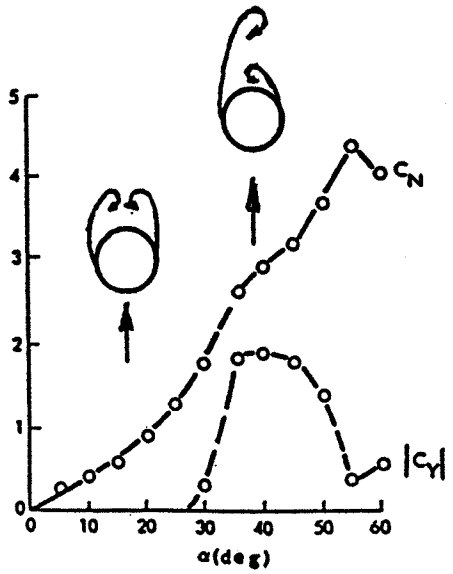

Fig. 18. Measured side force and normal force on a 5 caliber pointed tangent-ogive at Re = 0.3 x 10^6 (Ref. 20).

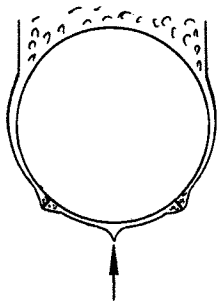

Fig. 19. Flow sketch of conceptual effect of body strakes on forebody crossflow at critical flow conditions.

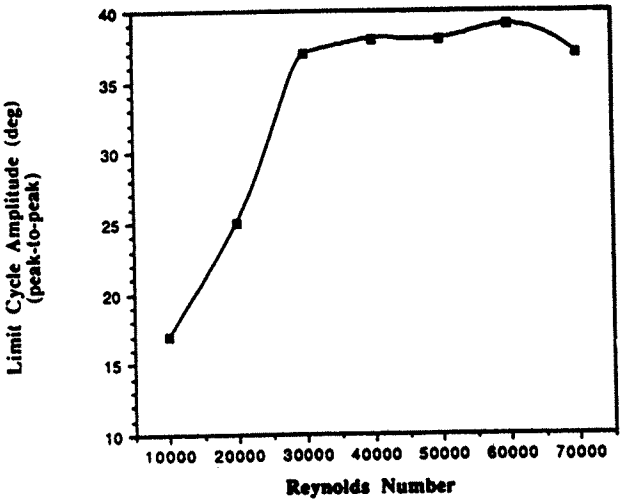

Fig. 21. F-18 LEX vortex breakdown location from flight and ground tests[10].

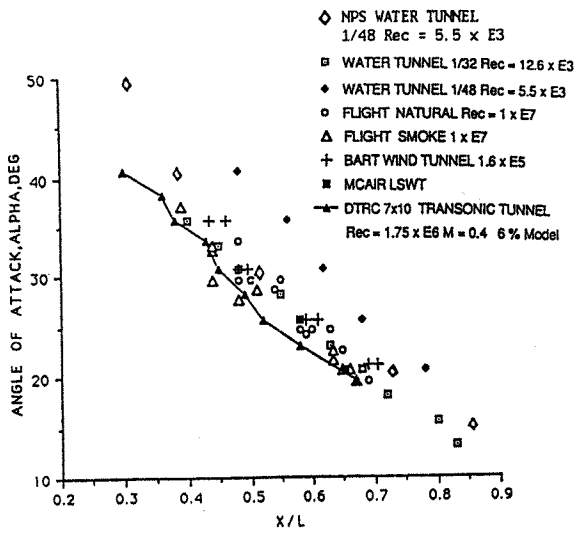

Fig. 20. Effect of Reynolds number on the wing rock of F-18 aircraft model at α = 45 deg[2].